Substrate-independent energy-level pinning of an organic semiconductor provides versatile hole-injection electrodes

Tianshu Zhai[1], Rongbin Wang[1,2], Takayoshi Katase[3,4], Frances Quigley[5], Hiromichi Ohta[6], Patrick Amsalem[2], Norbert Koch[1,2,7] and Steffen Duhm[1,*]

[1]*Institute of Functional Nano & Soft Materials (FUNSOM), Jiangsu Key Laboratory for Carbon-Based Functional Materials & Devices and Joint International Research Laboratory of Carbon-Based Functional Materials and Devices, Soochow University, Suzhou 215123, People's Republic of China*
[2]*Institut für Physik & IRIS Adlershof, Humboldt-Universität zu Berlin, 12489 Berlin, Germany*
[3]*Laboratory for Materials and Structures and Institute of Innovative Research, Tokyo Institute of Technology, Yokohama 226−8503, Japan*
[4]*PRESTO, Japan Science and Technology Agency, Tokyo 102-0076, Japan*
[5]*Trinity College Dublin, The University of Dublin, Dublin 2, Ireland*
[6]*Research Institute for Electronic Science, Hokkaido University, Sapporo 001-0020, Japan*
[7]*Helmholtz-Zentrum Berlin für Materialien und Energie GmbH, 12489 Berlin, Germany*
*duhm@suda.edu.cn

Tailor-made electrode work functions are indispensable to control energy-level offsets at the interfaces of (opto-)electronic devices. We show by means of photoelectron spectroscopy that several nm thick layers of the organic semiconductor 1,4,5,8,9,12-hexaaza-triphenylene-2,3,6,7,10,11-hexacarbonitrile (HAT-CN) on virtually all substrates provide hole-injecting electrodes with work functions of around 5.60 eV. This substrate-independent energy-level alignment can be traced back to a relatively large density of gap states in HAT-CN thin films, which, furthermore, make the wide-gap semiconductor thin films sufficiently conductive for electrode applications. Moreover, our study highlights a quite intriguing energy-level alignment scenario as the Fermi-level in HAT-CN thin films is located far from mid-gap position, which is rather uncommon for undoped organic semiconductor thin films.

Introduction

The performance of multilayer organic (opto-)electronic devices is controlled by their ubiquitous interfaces. In particular, energy-level offsets determine the effectiveness of charge generation and dissociation [1, 2, 3, 4, 5, 6]. Typical layer thicknesses in devices are in the range of few nm up to several 100 nm [2, 7, 8] and, in general, the energy-level alignment of such organic thin films with inorganic substrates is well understood [9, 10, 11]. Figure 1a shows, as an example, measured organic thin film work function values of the often used hole-transport material N,N-bis(1-naphthyl)-N,N-diphenyl-1,1-biphenyl-4,4-diamine (NPB) on various substrates [12, 13, 14]. For substrate work function (Φ) values below 4.80 eV the energy-level alignment is vacuum-level controlled and the thin film work function depends linearly on Φ. For larger substrate Φ, the thin film work function becomes independent of Φ, i.e., Fermi-level pinning takes place [12]. Remarkably, Fermi-level pinning does not concur when Φ and the ionization energy (IE) of NPB (5.35 eV) [12] have the same value, but occurs already earlier. Consequently, the highest occupied molecular orbital (HOMO) level of NPB is pinned at ca. 300 meV below the Fermi-level (E_F) (Figure 1b). This is related to energetic disorder in NPB thin films, which leads to a broadening of the HOMO-related density of states (DOS). This behavior of NPB is common for many organic semiconductors and in ultraviolet photoelectron spectroscopy (UPS) spectra of pinned systems the leading edge of the HOMO-derived peak can be usually found several hundred meV below the Fermi-level [15, 9, 10, 16, 17]. The same mechanism applies to pinning at the lowest unoccupied molecular orbital (LUMO) level above E_F. However, because the electron affinity (EA) of commonly used organic semiconductor thin films (e.g., 2.10 eV for NPB [18]) is often much lower than Φ of typical electrodes, pinning at the LUMO is less frequently observed [19].

In contrast, thin films of some organic semiconductors do not follow this typical energy-level alignment scheme, prominent examples are 2,3,5,6-tetrafluoro-7,7,8,8 tetracyanoquino-dimethane (F4-TCNQ) [20] and 3,4,9,10-perylene-tetracarboxylic-dianhydride (PTCDA) [21]. Thin films of these materials show Fermi-level pinning for a very wide range of substrate Φ (Figure 1). For PTCDA this was recently related to substrate induced broadening of energy-levels and/or gap states [21]. For similar systems, alternative mechanisms have been proposed to explain the energy-level alignment, such as integer charge transfer (ICT) induced states [15, 20] or induced density of interface states (IDIS) [22, 23, 24]. However, a general description of such substrate-independent pinning (SIP)

is still missing, although SIP is beneficial for many electronic applications, because a layer of a material showing SIP will exhibit the same work function on any substrate and, thus, allows facile charge-injection barrier tuning of subsequently deposited layers [25, 26, 27]. PTCDA has not found wide application for energy-level engineering purposes as the substrate independent work function is around 4.60 eV (Figure 1a) [21, 28], which is neither a particularly large nor low work function and, thus, PTCDA thin films are neither superior for hole nor electron injection. F4-TCNQ thin films have a rather high work function of around 5.55 eV (Figure 1a) [20] and provide good hole-injecting electrodes. However, possible device application is hampered by diffusion of F4-TCNQ, due to its relatively low molecular weight, through organic layers [29, **Fehler! Verweisquelle konnte nicht gefunden werden.**, 31, 32, 33]. It has been suggested that larger molecules like 1,4,5,8,9,12-hexaaza-triphenylene-2,3,6,7,10,11-hexacarbonitrile (HAT-CN), are less prone to diffusion [29, 34, 35, 36]. Moreover, HAT-CN thin films provide a hole injection electrode with a work function of around 5.50 eV [13, 37, 38, 39, 40] and are, hence, frequently used in organic optoelectronic devices [39, 41, 42, 43, 44, 45, 46, 47]. HAT-CN can be easily processed by thermal evaporation at low temperature, making it possible to replace commonly used hole injection materials like molybdenum trioxide (MoO_3) [48, 49] or tungsten trioxide (WO_3) [50]. HAT-CN thin films have IEs of around 9.50 eV [38, 40, 51, 52, 53, 54, 55] and the transport gap is 4.20 eV [56]. The Fermi-level of HAT-CN is typically pinned 0.50 eV below the LUMO and, consistently with the bandgap, the HOMO lies about 4 eV from the Fermi-level (Figure 1b). However, pinning was reported on substrates covering a narrow work function range (between 3.50 eV and 4.60 eV) [37, 38, 39, 40], which does not allow to unequivocally conclude whether HAT-CN thin films actually show SIP.

To address the question whether SIP is the mechanism leading to the high work function of HAT-CN films, we employed UPS and X-ray photoelectron spectroscopy (XPS) for HAT-CN on substrates covering a much wider Φ range. For this purpose, VO_{2-x} is very well suited, as its Φ can be tuned from 4.40 eV to 6.70 eV by controlling the density of oxygen vacancies [57]. To provide for more general insight, MoO_3 with a high work function of 7.00 eV [58, 59] was used and Au(111) served as a reference substrate due to its moderate work function of 5.50 eV [60]. Our results show that E_F-pinning prevails even for substrate work function as high as 7.00 eV (Figure 1) and HAT-CN thin films exhibit, indeed, SIP with Φ of 5.60 ± 0.15 eV. Notably, UPS reveals the presence of gap states between the HOMO-level and the Fermi-level, which explain the mechanism of SIP for HAT-CN on virtually any substrate.

Experimental Details

VO$_2$ substrates were fabricated by pulsed laser deposition (PLD) on sapphire [61]. The preparation steps of stoichiometric VO$_2$ and oxygen deficient VO$_{2-x}$ can be found in our previous work [57]. MoO$_x$ was purchased from Strem Chemicals (purity of 99.5%) and thermally evaporated onto indium-tin-oxide (ITO, nominal thickness: 200 Å). The Au(111) substrate was cleaned by series of annealing (at 650 K) and Ar$^+$ ion bombardment. Unless noted otherwise, experiments were performed with HAT-CN, which was purchased from Aladdin with a purity of 99% (HPLC). HAT-CN molecules were thermally deposited inside an ultra-high vacuum (UHV) chamber with a base pressure of 2 × 10^{-10} mbar. The nominal mass thickness was monitored by a quartz crystal microbalance. For PES measurements the samples were transferred to an analysis chamber (base pressure: 1 × 10^{-10} mbar) without breaking UHV conditions. UPS measurements were performed using the monochromatized He I$_\alpha$ line (21.22 eV) and XPS measurements with monochromatized Al K$_\alpha$ radiation (1486.7 eV). All measurements were conducted at room temperature (295 K). The energy scale in the plots of the secondary electron regions is corrected by the applied bias voltage and the analyzer work function. Thus, the position of the secondary electron cutoff (SECO) corresponds to the thin film work function. The deconvolution of core level spectra is conducted using Voigt peaks and a Shirley background. The C1s and N1s relative sensitivity factors were applied to calculate the relative atomic ratios [62].

Results and Discussion

The VO$_2$ and VO$_{2-x}$ substrates have work function values of 6.72 eV and 4.59 eV, respectively (Figure 2). Besides this difference, the substrates only differ in the density of oxygen vacancies, which induces variation in the valence electronic structure [57]. Figure 2 shows UPS and XPS spectra of the bare substrates and with HAT-CN layers with nominal thicknesses of 8 Å and 128 Å; spectra with intermediate HAT-CN thicknesses can be found in the Supporting Information (Figure S2 and S3). Strikingly, for multilayer HAT-CN coverage (nominally 128 Å), besides minor shifts (less than 0.21 eV) in absolute binding energy (BE) of the core- and HOMO-levels, the spectra are virtually identical albeit the initial substrate work function differs by 2.13 eV, and it is lower (VO$_{2-x}$) *and* higher (VO$_2$) than the common work function of HAT-CN thin films.

Deposition of a nominal 8 Å thick HAT-CN film on low Φ VO$_{2-x}$ increases the work function to 5.60 eV and then decreases slightly by 0.25 eV for 128 Å (Figure 2c and Figure S4a). The initial increase of the work function can be ascribed to an electron transfer (CT) from VO$_{2-x}$ to HAT-CN, as the HAT-CN EA of 5.40 eV (as measured by inverse photoemission) [39] is higher than Φ of VO$_{2-x}$. Thus, in case of vacuum-level

alignment, the LUMO-level of HAT-CN would be found below E_F, which corresponds to an electronic non-equilibrium situation. Through CT, the LUMO of HAT-CN becomes occupied and the resulting interface dipole leads to the increase of the work function. Unfortunately, the partially filled LUMO near the Fermi level cannot be clearly distinguished in the UPS spectra due to the overlap with the valence bands of the VO_{2-x} substrate, but it has already been reported previously for other HAT-CN/substrate interfaces [56]. The mentioned small, yet important, lowering of the work function for multilayer coverage is discussed further below. The valence spectra of multilayer HAT-CN on VO_{2-x} (Figure 2b) are virtually identical to those in multilayers on other substrates [13, 37, 40]. In particular, the IE (9.65 eV), as determined by the work function and the low BE onset of the HOMO-derived peak, matches previously reported values between 9.5 eV to 9.8 eV [56, 63, 64, 40]. In the C1s XPS spectra (Figure 2d) the chemical shift between carbon atoms in an aromatic environment (CN) and those in the cyano groups (C≡N) is apparent. For multilayer coverage, they are centered at 287.20 eV BE and 287.80 eV BE, respectively. At 8 Å nominal thickness two additional peaks on the low BE side are necessary to fit the spectra. These features are assigned to negatively charged HAT-CN [13, 40] and they are dominated by the signal from the cyano groups, which accommodate more electron density due to CT. The N1s peaks also show CT features for 8 Å HAT-CN thickness (Figure 2e), and for thicknesses of 32 Å or higher only the neutral species are present (Figure S3 in Supporting Information). Overall, the presence of charged molecules at the interface of HAT-CN and VO_{2-x} is in line with previous reports of HAT-CN on other low work function substrates [13, 37, 40].

Deposition of 8 Å HAT-CN on high Φ VO_2 decreases the work function to 6.00 eV and Φ decreases further to 5.83 eV for a thickness of 128 Å (Figure 2c). Assuming vacuum-level alignment would occur, the Fermi-level would come to lie well within the gap of HAT-CN, which would correspond to an electronic equilibrium situation and no CT (and no change of Φ) should occur. Therefore, the Φ change (and associated CT) must have a different origin than what we concluded on for HAT-CN on low Φ VO_{2-x}. Similarly, no CT features can be observed in XPS (Figure 2d and 2e). A part of the initial work-function change could be related to the electronic push-back effect, which usually takes place upon molecular deposition on clean metal surfaces [65, 66, 67] and conductive oxides like indium-tin-oxide [68]. However, the push-back effect will only result in an abrupt interface dipole, i.e., no further Φ change after monolayer formation. In contrast, both an initial rapid change of the work function (0.89 eV) as well as a continuous shift of the HOMO-level and core-levels (0.78 eV) with increasing HAT-CN coverage on VO_2 is observed (Figure S2, S3 and S4 in

Supporting Information) [69, 70]. The latter is a tell-tale sign of energy-level bending [1, 71] and is indicative of SIP. Note that the difference between the Φ change ($\Delta\Phi$ =0.89 eV) and HOMO- and core-level shift (Δ_{core} =0.78 eV) is, due to the interface dipole because of the push-back effect.

To summarize these two experiments, the energy-level alignment of HAT-CN on low Φ VO_{2-x} can unambiguously be explained with E_F-pinning due to electron transfer from the valence bands of VO_{2-x} to the HAT-CN LUMO, to reach electronic equilibrium. However, the downward energy-level bending of HAT-CN on high Φ VO_2 cannot be simply explained by invoking electron transfer from HAT-CN HOMO to the conduction band minimum (CBM) of VO_2 because the HOMO of HAT-CN lies much deeper than the CBM of VO_2. Thus, the induced downward energy-level bending on high Φ VO_2 and suspected SIP must originate from another CT pathway, whose origin is elucidated in the following.

To substantiate that SIP occurs for HAT-CN thin films, we used another high Φ substrate, namely MoO_x. The low DOS of MoO_x between E_F and 3 eV BE (Figure 3a) makes it furthermore possible to track fine features in the region between the HAT-CN HOMO-onset (at 2.45 eV BE, for nominal HAT-CN thicknesses of 2 Å up to 32 Å) and the Fermi-level, also for low coverages. Strikingly, after deposition of 8 Å HAT-CN on MoO_x, a relatively large DOS (with a maximum around 1.00 eV BE) is observed in the energy gap of HAT-CN, which ranges from the Fermi-level to the HOMO-onset. By increasing the HAT-CN thickness to 192 Å, the HOMO and the gap states shift to higher BE and stay at constant BE for thicknesses up to 320 Å. Concomitantly, starting with a MoO_x Φ of 7.00 eV (Figure 3b), the work function is found to decrease to 6.67 eV for a HAT-CN thickness of 32 Å, and a further decrease to 5.70 eV is observed for thicknesses of 192 Å and beyond. The C1s spectra of HAT-CN on MoO_x (Figure S5a) show the usual double-peak structure as on the other substrates, and for low coverages no additional peaks are apparent. The overall C1s shift amounts to 1.25 eV, which is similar to the overall Φ change (1.40 eV). These observations point to a small interface dipole (~0.15 eV) and substantial energy-level bending (~1.25 eV) upon multilayer formation of HAT-CN on MoO_x (Figure S5 and S6 in the Supporting Information).

The energy-level bending within the HAT-CN layer on MoO_x can be readily explained by CT from these gap states [10]. Most importantly, the gap states are also clearly visible for multilayer coverage, i.e., they are *not* interface states. Moreover, they are visible on *all* substrates, as a close inspection of the log-scale plotted valence electron region of multilayer HAT-CN on all four substrates (Figure 3c) reveals their presence at ca. 3.00 eV and 1.50 eV BE. Moreover, the tail of the low BE peak

(centered at ca. 1.50 eV) extends down to 0.90 eV BE (most pronounced on MoO_x). Importantly, while the details of the DOS show slight differences, the large density of gap states in the bulk organic thin films can readily explain the occurrence of the SIP. The measurements on the high work function substrates and on Au(111) (Figure S7 in Supporting Information) confirm SIP of HAT-CN, and in all cases the work function approaches ~5.60 eV for multilayer films (Figure 1). The same holds for thin films prepared with HAT-CN powder from a different supplier (Figure S8). The gap states are also clearly visible in these spectra and their appearance does, thus, not possibly stem from a defective batch of molecules.

The mechanisms of SIP are visualized in the energy-level diagrams of HAT-CN on VO_{2-x}, on VO_2, and on MoO_x (Figure 4), where it becomes clear that the CT mechanisms are fundamentally different for low Φ and high Φ substrates. As discussed above, on low Φ VO_{2-x} (Figure 4a), electrons transfer from the valence bands of VO_{2-x} to the LUMO of HAT-CN to achieve electronic equilibrium, resulting in the formation of a predominant interface dipole (1.09 eV). This represents "regular" Fermi-level pinning, similar to other high EA organic molecules on low Φ substrates [9, 10, 11]. Most notably, after this increase of the work function (due to CT) on low Φ VO_{2-x}, the energy levels bend *downwards*, although the LUMO level is already much closer to E_F than the HOMO level. This is interpreted as a result of the competing CT mechanism from the gap states of HAT-CN to the conduction band of VO_{2-x}, leading to SIP. On high Φ VO_2 (Figure 4b) and MoO_x (Figure 4c), electron transfer from the HOMO of HAT-CN to the CBM of VO_2 or MoO_x can be dismissed on common grounds. The appropriate manner to account for the energy level alignment is that of an electron transfer from the occupied density of gap states to the CBM of VO_2 or MoO_x. Thus, we infer that the SIP of HAT-CN on high Φ substrates is caused by the proximity in energy between these gap states and the HAT-CN LUMO, resulting in almost constant HAT-CN multilayer Φ of around 5.60 eV, with only small sample- and substrate-dependent variations. Therefore, it follows that HAT-CN, which is commonly regarded as a strong electron *acceptor* due to its high EA, is also able to *donate* electrons to high Φ substrates due to the presence of a significant occupied gap state density.

Conclusion

Our work provides evidence for substrate-independent pinning of HAT-CN thin films. The work function of these thin films is ca. 5.60 eV and they provide robust functional hole-injection layers for (opto-)electronic applications. The peculiar energy-level

alignment of HAT-CN thin films can be explained by the proximity in energy between the LUMO and a large density of occupied gap states which also prevails for multilayer coverage. The gap states are found almost independent of the provider of the HAT-CN powder and are, most likely, related to inherent chemical defects, whose origin should be unraveled in further studies. In any case, the predictable behavior of HAT-CN on a variety of substrates appears as a key advantage for turning low Φ substrates into hole injecting electrodes, but also to act as a protective buffer layer with constant work function for sensitive substrates, exemplified here with VO_{2-x}, which exhibits tremendous change in work function by only slight changes in surface composition.

References

[1] H. Ishii, K. Sugiyama, E. Ito, and K. Seki. Energy level alignment and interfacial electronic structures at organic/metal and organic/organic interfaces. *Adv. Mater.*, 11:605-625, 1999.

[2] N. Koch. Organic Electronic Devices and Their Functional Interfaces. *Chem. Phys. Chem.*, 8:1438-1455, 2007.

[3] Kouki Akaike. Distributions of potential and contact-induced charges in conventional organic photovoltaics. *Materials*, 13(10):2411, 2020.

[4] X. Wu, R. Jia, J. Pan, X. Zhang, and J. Jie. Roles of interfaces in the ideality of organic field-effect transistors. *Nanoscale Horiz*, 5(3):454-472, 2020.

[5] M. Waldrip, O. D. Jurchescu, D. J. Gundlach, and E. G. Bittle. Contact resistance in organic field-effect transistors: Conquering the barrier. *Adv. Funct. Mater.*, 30(20):1904576, 2019.

[6] M. Fahlman, S. Fabiano, V. Gueskine, D. Simon, M. Berggren, and X. Crispin. Interfaces in organic electronics. *Nat. Rev. Mater.*, 4:627-650, 2019.

[7] C. W. Tang. Two-layer organic photovoltaic cell. *Appl. Phys. Lett.*, 48:183-185, 1986.

[8] V. G. Kozlov, V. Bulović, P. E. Burrows, and S. R. Forrest. Laser action in organic semiconductor waveguide and double-heterostructure devices. *Nature*, 389(6649):362-364, 1997.

[9] M. Oehzelt, N. Koch, and G. Heimel. Organic semiconductor density of states controls the energy level alignment at electrode interfaces. *Nat. Commun.*, 5:4174-8, 2014.

[10] J.-P. Yang, F. Bussolotti, S. Kera, and N. Ueno. Origin and role of gap states in organic semiconductor studied by UPS: as the nature of organic molecular crystals. *J. Phys. D: Appl. Phys.*, 50:423002, 2017.

[11] L. Ley, Y. Smets, C. I. Pakes, and J. Ristein. Calculating the universal energy-level alignment of organic molecules on metal oxides. *Adv. Funct. Mater.*, 23:794-805, 2013.

[12] S. Braun, W. Osikowicz, Y. Wang, and W. R. Salaneck. Energy level alignment regimes at hybrid organic-organic and inorganic-organic interfaces. *Org. Electron.*, 8:14-20, 2007.

[13] E. Oh, S. Park, J. Jeong, S. J. Kang, H. Lee, and Y. Yi. Energy level alignment at the interface of NPB/HAT-CN/graphene for flexible organic light-emitting diodes. *Chem. Phys. Lett*, 668:64-68, 2017.

[14] L. Li, X. Liu, L. Lyu, R. Wu, P. Liu, Y. Zhang, Y. Zhao, H. Wang, D. Niu, J. Yang, and Y. Gao. Modification of ultrathin npb interlayer on the electronic structures of the ch3nh3pbi3/npb/moo3 interface. *J. Phys. Chem. C*, 120(32):17863-17871, 2016.

[15] S. Braun, W. R. Salaneck, and M. Fahlman. Energy-level alignment at organic/metal and organic/organic interfaces. *Adv. Mater.*, 21:1450-1472, 2009.

[16] H. Fukagawa, S. Kera, T. Kataoka, S. Hosoumi, Y. Watanabe, K. Kudo, and N. Ueno. Role of ionization potential in vacuum-level alignment at organic semiconductors interfaces. *Adv. Mater.*, 19:665-668, 2007.

[17] G. Horowitz. Validity of the concept of band edge in organic semiconductors. *J. Appl. Phys.*, 118:115502-5, 2015.

[18] S. Y. Liu, J. H. Chang, I. W. Wu, and C. I. Wu. Alternating current driven organic light emitting diodes using lithium fluoride insulating layers. *Sci. Rep.*, 4(1), 2014.

[19] P. Hurdax, M. Hollerer, P. Puschnig, D. Lüftner, L. Egger, M. G. Ramsey, and M. Sterrer. Controlling the charge transfer across thin dielectric interlayers. *Adv. Mater. Interfaces*, 2000592, 2020.

[20] S. Braun and W. R. Salaneck. Fermi level pinning at interfaces with tetrafluoro tetracyano quinodimethane (F4-TCNQ): The role of integer charge transfer states. *Chem. Phys. Lett.*, 438:259-262, 2007.

[21] M. S. Khoshkhoo, H. Peisert, T. Chasse, and M. Scheele. The role of the density of interface states in interfacial energy level alignment of PTCDA. *Org. Electron.*, 49:249-254, 2017.

[22] H. Hasegawa and H. Ohno. Unified disorder induced gap state model for insulator-semiconductor and metal-semiconductor interfaces. *J. Vac. Sci. Technol. B*, 4(4):1130-1138, 1986.

[23] H. Vázquez, F. Flores, and A. Kahn. Induced density of states model for weakly-interacting organic semiconductor interfaces. *Org. Electron.*, 8(2-3):241-248, 2007.

[24] S. Yogev, R. Matsubara, M. Nakamura, U. Zschieschang, H. Klauk, and Y. Rosenwaks. Fermi level pinning by gap states in organic semiconductors. *Phys. Rev. Lett.*, 110:036803-5, 2013.

[25] N. Koch, S. Duhm, J. P. Rabe, A. Vollmer, and R. L. Johnson. Optimized hole injection with strong electron acceptors at organic-metal interfaces. *Phys. Rev. Lett.*, 95:237601-4, 2005.

[26] F. Widdascheck, A. A. Hauke, and G. Witte. A Solvent-Free Solution: Vacuum-Deposited Organic Monolayers Modify Work Functions of Noble Metal Electrodes. *Adv. Funct. Mater.*, 29:1808385-10, 2019.

[27] E. Zojer, T. C. Taucher, and O. T. Hofmann. The Impact of Dipolar Layers on the Electronic Properties of Organic/Inorganic Hybrid Interfaces. *Adv. Mater. Interfaces*, 6:1900581-32, 2019.

[28] S. Duhm, A. Gerlach, I. Salzmann, B. Bröker, R. L. Johnson, F. Schreiber, and N. Koch. PTCDA on Au(111), Ag(111) and Cu(111): Correlation of interface charge transfer to bonding distance. *Org. Electron.*, 9:111-118, 2008.

[29] I. E. Jacobs and A. J. Moulé. Controlling molecular doping in organic semiconductors. *Adv. Mater.*, 29:1703063-39, 2017.

[30] J. Li, C. W. Rochester, I. E. Jacobs, S. Friedrich, P. Stroeve, M. Riede, and A. J. Moule. Measurement of Small Molecular Dopant F4-TCNQ and $C_{60}F_{36}$ Diffusion in Organic Bilayer Architectures. *ACS Appl. Mater. Interfaces*, 7:28420-28428, 2015.

[31] I. Bruder, S. Watanabe, J. Qu, I. B. Müller, R. Kopecek, J. Hwang, J. Weis, and N. Langer. A novel p-dopant with low diffusion tendency and its application to organic light-emitting diodes. *Org. Electron.*, 11:589-593, 2010.

[32] S. Duhm, I. Salzmann, B. Bröker, H. Glowatzki, R. L. Johnson, and N. Koch. Interdiffusion of molecular acceptors through organic layers to metal substrates mimics doping-related energy level shifts. *Appl. Phys. Lett.*, 95:093305, 2009.

[33] P. Tyagi, M. Kumar Dalai, C. K. Suman, S. Tuli, and R. Srivastava. Study of 2,3,5,6-tetrafluoro-7,7',8,8'-tetracyano quinodimethane diffusion in organic light emitting diodes using secondary ion mass spectroscopy. *RSC Adv.*, 3:24553-24559, 2013.

[34] L. Zhang, F. S. Zu, Y. L. Deng, F. Igbari, Z. K. Wang, and L. S. Liao. Origin of Enhanced Hole Injection in Organic Light-Emitting Diodes with an Electron-Acceptor Doping Layer: p-Type Doping or Interfacial Diffusion? *ACS Appl. Mater. Interfaces*, 7:11965-11971, 2015.

[35] P. Amsalem, A. Wilke, J. Frisch, J. Niederhausen, A. Vollmer, R. Rieger, K. Müllen, J. P. Rabe, and N. Koch. Interlayer molecular diffusion and thermodynamic equilibrium in organic heterostructures on a metal electrode. *J. Appl. Phys.*, 110:113709-6, 2011.

[36] M. H. Futscher, T. Schultz, J. Frisch, M. Ralaiarisoa, E. Metwalli, M. V. Nardi, P. Müller-Buschbaum, and N. Koch. Electronic properties of hybrid organic/inorganic semiconductor pn-junctions. *J. Phys.: Condens. Matter*, 31:064002-8, 2019.

[37] F. Zu, P. Amsalem, M. Ralaiarisoa, T. Schultz, R. Schlesinger, and N. Koch. Surface State Density Determines the Energy Level Alignment at Hybrid Perovskite/Electron Acceptors Interfaces. *ACS Appl. Mater. Interfaces*, 9:41546-41552, 2017.

[38] J.-P. Yang, F. Bussolotti, Y.-Q. Li, X.-H. Zeng, S. Kera, J.-X. Tang, and N. Ueno. The role of gap states on energy level alignment at an alpha-NPD/HAT(CN)$_6$ charge generation interface. *Org. Electron.*, 24:120-124, 2015.

[39] S. Lee, J.-H. Lee, J.-H. Lee, and J.-J. Kim. The mechanism of charge generation in charge-generation units composed of p-doped hole-transporting layer/HATCN/n-doped electron-transporting layers. *Adv. Funct. Mater.*, 22:855-860, 2012.

[40] C. Christodoulou, A. Giannakopoulos, M. V. Nardi, G. Ligorio, M. Oehzelt, L. Chen, L. Pasquali, M. Timpel, A. Giglia, S. Nannarone, P. Norman, M. Linares, K. Parvez, K. Müllen, D. Beljonne, and N. Koch. Tuning the work function of graphene-on-quartz with a high weight molecular acceptor. *J. Phys. Chem. C*, 118:4784-4790, 2014.

[41] R.-B. Wang, Q.-K. Wang, H.-J. Xie, L.-H. Xu, S. Duhm, Y.-Q. Li, and J.-X. Tang. Hatcn-based charge recombination layers as effective interconnectors for tandem organic solar cells. *ACS Appl. Mater. Interfaces*, 6:15604-15609, 2014.

[42] E. Najafabadi, K. A. Knauer, W. Haske, and B. Kippelen. High-performance inverted top-emitting green electrophosphorescent organic light-emitting diodes with a modified top ag anode. *Org. Electron.*, 14:1271-1275, 2013.

[43] L.-S. Liao, W.-K. Slusarek, T.-K. Hatwar, M.-L. Ricks, and D.-L. Comfort. Tandem Organic Light-Emitting Diode using Hexaazatriphenylene Hexacarbonitrile in the Intermediate Connector. *Adv. Mater.*, 20:324-329, 2008.

[44] C. Falkenberg, S. Olthof, R. Rieger, M. Baumgarten, K. Muellen, K. Leo, and M. Riede. The role of energy level matching in organic solar cells hexaazatriphenylene hexacarbonitrile as transparent electron transport material. *Sol. Energ. Mater. Sol. C.*, 95(3):927-932, 2011.

[45] H Zhang, S. Chen, and X. Sun. Efficient red/green/blue tandem quantum-dot light-emitting diodes with external quantum efficiency exceeding 21%. *ACS Nano*, 12(1):697-704, 2018.

[46] K. Kuwano, H. Ogo, M. Chikamatsu, Y. Yoshida, Y. Watanabe, and E. Nishikawa. Effects on p-type buffer layers for semitransparent organic photovoltaics using indium zinc oxide transparent electrode. *Jpn. J. Appl. Phys.*, 59(SD):SDDD04, 2019.

[47] J. Chen, K. Wang, X. Ma, C. Dong, Y. Zhang, X. Li, and Z. Wang. Enhancement of stability by applying HAT-CN for hole modification with good water resistance and hole extraction. *IEEE J. Photovolt.*, 10(4):1023–1026, 2020.

[48] M. Kröger, S. Hamwi, J. Meyer, T. Riedl, W. Kowalsky, and A. Kahn. Role of the deep-lying electronic states of MoO_3 in the enhancement of hole-injection in organic thin films. *Appl. Phys. Lett.*, 95(12):123301, 2009.

[49] R. Wang, Y. Wang, C. Wu, T. Zhai, J. Yang, B. Sun, S. Duhm, and N. Koch. Direct observation of the inversion layer between PEDOT:PSS and n-Si(100) by photoelectron spectroscopy. *Adv. Funct. Mater.*, 30(4): 1903440, 2020.

[50] M. Bivour, J. Temmler, H. Steinkemper, and M. Hermle. Molybdenum and tungsten oxide: High work function wide band gap contact materials for hole selective contacts of silicon solar cells. *Sol. Energy Mater. Sol. Cells*, 142:34–41, 2015.

[51] J. Niederhausen, P. Amsalem, J. Frisch, A. Wilke, A. Vollmer, R. Rieger, K. Müllen, J. P. Rabe, and N. Koch. Tuning hole-injection barriers at organic/metal interfaces exploiting the orientation of a molecular acceptor interlayer. *Phys. Rev. B*, 84:165302–, 2011.

[52] A. L. Shi, Y. Q. Li, X. C. Jiang, Z. S. Ma, Q. K. Wang, Z.-Y. Guo, D. D. Zhang, S. T. Lee, and J. X. Tang. A low-temperature processed environment-friendly full-organic carrier collection layer for polymer solar cells. *Appl. Phys. Lett.*, 105(5):053305, 2014.

[53] J. Jeong, S. Park, S. J. Kang, H. Lee, and Y. Yi. Impacts of molecular orientation on the hole injection barrier reduction: CuPC/HAT-CN/graphene. *J. Phys. Chem. C*, 120(4):2292-2298, 2016.

[54] P. S. Johnson, I. Boukahil, F. J. Himpsel, K. L. Kearns, J. H. Kang, J.C. Lin, A. Leugers, G. Meyers, S. Mukhopadhyay, D. H. K. Jackson, and T. F. Kuech. Multi-technique approach for determining energy levels and exciton binding energies of molecules for organic electronics. *J. Phys. Chem. C*, 120(3):1366-1374, 2016.

[55] K. Müller, N. Schmidt, S. Link, R. Riedel, J. Bock, W. Malone, K. Lasri, A. Kara, U. Starke, M. Kivala, and M. Stöhr. Triphenylene-derived electron acceptors and donors on Ag(111): Formation of intermolecular charge-transfer complexes with common unoccupied molecular states. *Small*, 15(33):1901741, 2019.

[56] H. Lee, J. Lee, S. Park, Y. Yi, S. W. Cho, J. W. Kim, and S. J. Kang. Hole injection enhancement of a single-walled carbon nanotube anode using an organic charge-generation layer. *Carbon*, 71:268–275, 2014.

[57] R. Wang, T. Katase, K.-K. Fu, T. Zhai, J. Yang, Q. Wang, H. Ohta, N. Koch, and S. Duhm. Oxygen Vacancies Allow Tuning the Work Function of Vanadium Dioxide. *Adv. Mater. Interfaces*, 5:1801033–7, 2018.

[58] Y. Z. Guo and J. Robertson. Origin of the high work function and high conductivity of moo3. *Appl. Phys. Lett.*, 105(22):222110, 2014.

[59] M. T. Greiner, L. Chai, M. G. Helander, W. M. Tang, and Z. H. Lu. Metal/metal-oxide interfaces: How metal contacts affect the work function and band structure of moo3. *Adv. Funct. Mater.*, 23(2):215–226, 2013.

[60] M.-C. Lu, R.-B. Wang, A. Yang, and S. Duhm. Pentacene on Au(111), Ag(111) and Cu(111): From physisorption to chemisorption. *J. Phys.: Condens. Matter*, 28:094005–9, 2016.

[61] T. Katase, K. Endo, and H. Ohta. Thermopower analysis of metal-insulator transition temperature modulations in vanadium dioxide thin films with lattice distortion. *Phys. Rev. B*, 92:035302, 2015.

[62] J. F. Moulder, W. F. Stickle, P. E. Sobol, and K. D. Bomben. *Handbook of X-ray Photoelectron Spectroscopy*. Physical Electronics, Inc., 1995.

[63] S. Lee, J.-H. Lee, K. H. Kim, S.-J. Yoo, T. G. Kim, J. W. Kim, and J.-J. Kim. Determination of the interface energy level alignment of a doped organic hetero-junction using capacitance-voltage measurements. *Org. Electron.*, 13:2346-2351, 2012.

[64] S. M. Park, Y. H. Kim, Y. Yi, H.-Y. Oh, and J. W. Kim. Insertion of an organic interlayer for hole current enhancement in inverted organic light emitting devices. *Appl. Phys. Lett.*, 97(6):063308, 2010.

[65] V. De Renzi, R. Rousseau, D. Marchetto, R. Biagi, S. Scandolo, and U. del Pennino. Metal work-function changes induced by organic adsorbates: A combined experimental and theoretical study. *Phys. Rev. Lett.*, 95(4), 2005.

[66] P. C. Rusu, G. Giovannetti, C. Weijtens, R. Coehoorn, and G. Brocks. First-principles study of the dipole layer formation at metal-organic interfaces. *Phys. Rev. B*, 81:125403-17, 2010.

[67] M. Bokdam, G. Brocks, and P. J. Kelly. Large potential steps at weakly interacting metal-insulator interfaces. *Phys. Rev. B*, 90(20), 2014.

[68] S. Winkler, J. Frisch, R. Schlesinger, M. Oehzelt, R. Rieger, J. Räder, J. P. Rabe, K. Müllen, and N. Koch. The impact of local work function variations on fermi level pinning of organic semiconductors. *J. Phys. Chem. C*, 117:22285-22289, 2013.

[69] T. Schultz, T. Lenz, N. Kotadiya, G. Heimel, G. Glasser, R. Berger, P. W. M. Blom, P. Amsalem, D. M. de Leeuw, and N. Koch. Reliable Work Function Determination of Multicomponent Surfaces and Interfaces: The Role of Electrostatic Potentials in Ultraviolet Photoelectron Spectroscopy. *Adv. Mater. Interfaces*, 4:1700324-8, 2017.

[70] T. Schultz, P. Amsalem, N. B. Kotadiya, T. Lenz, P. W. M. Blom, and N. Koch. Importance of Substrate Work Function Homogeneity for Reliable Ionization Energy Determination by Photoelectron Spectroscopy. *Phys. Status. Solidi. B*, 256:1800299-6, 2019.

[71] H Ishii, H Oji, E Ito, N Hayashi, D Yoshimura, and K Seki. Energy level alignment and band bending at model interfaces of organic electroluminescent devices. *J. Lumin.*, 87-89:61-65, 2000.

Figures
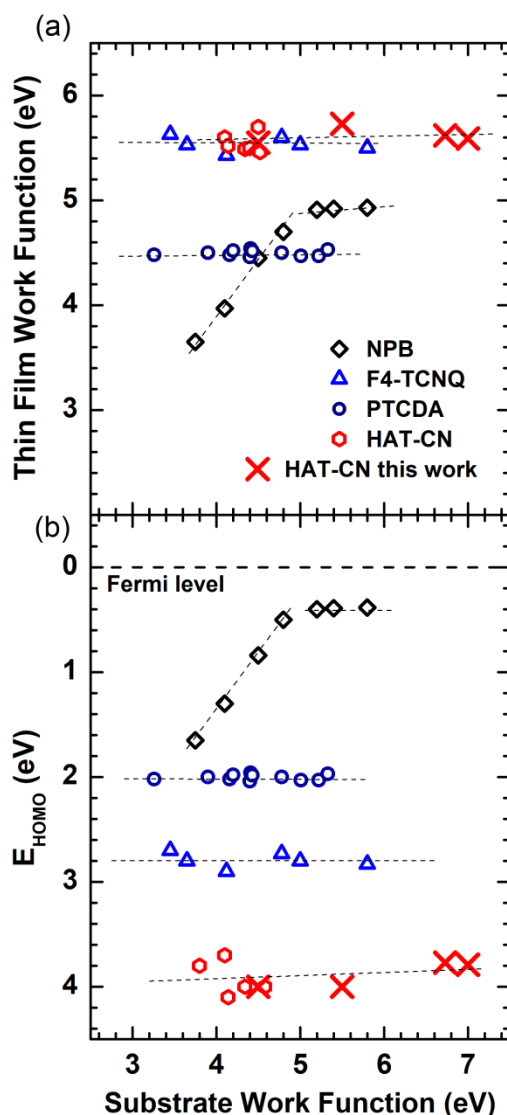
Figure 1 a) Thin film work function values and b) thin film HOMO-levels below the Fermi-level (E_F) of common organic semiconductors as function of substrate work function. The values for NPB (black diamonds), F4-TCNQ (blue triangles), and PTCDA (navy circles are taken from literature [12, 20, 21]. The values of HAT-CN (red empty hexagons) are taken from literature [37, 38, 39, 40] and our own work (red crosses). Dash lines serve as guides to the eye.
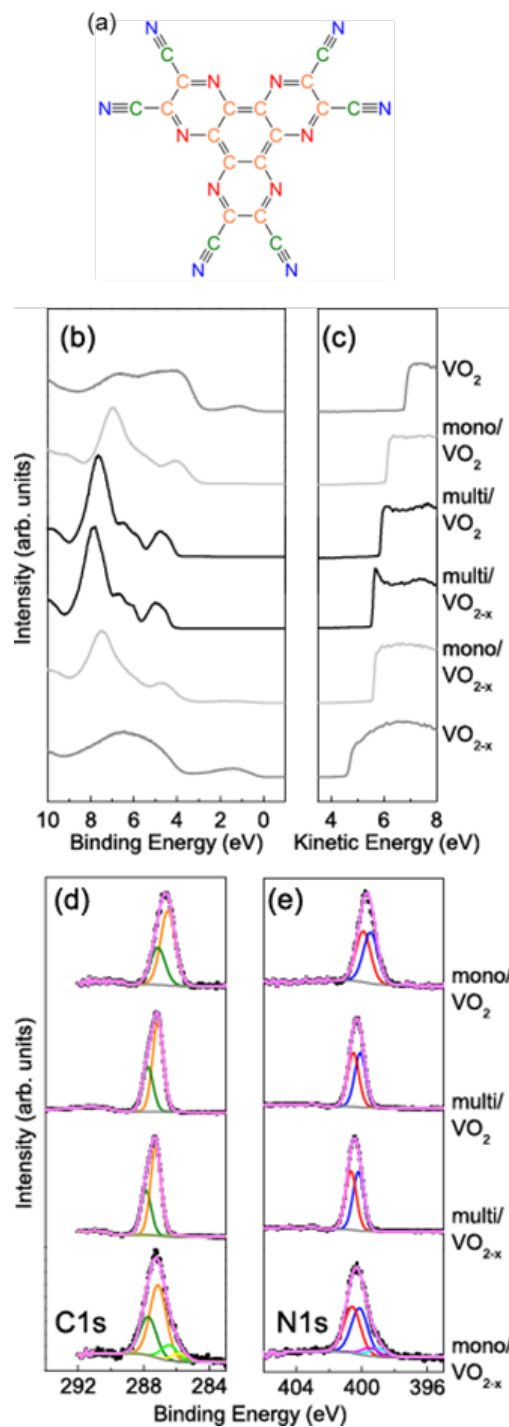
Figure 2 The chemical structure of HAT-CN (a) shows color coded atom species: The nitrogen and carbon atoms in the cyano group C≡N are colored in violet and green, respectively. The nitrogen and carbon atoms in aromatic ring are colored in red and orange, respectively. Valence band (b) and SECO (c) region of UPS spectra of VO_{2-x} and VO_2 substrates and HAT-CN thin films with nominal thicknesses of 8 Å (mono) and 128 Å (multi). XPS spectra of C1s core level (d) and N1s core level (e) of HAT-CN thin films. The same color code as in (a) applies for the fits of XPS.
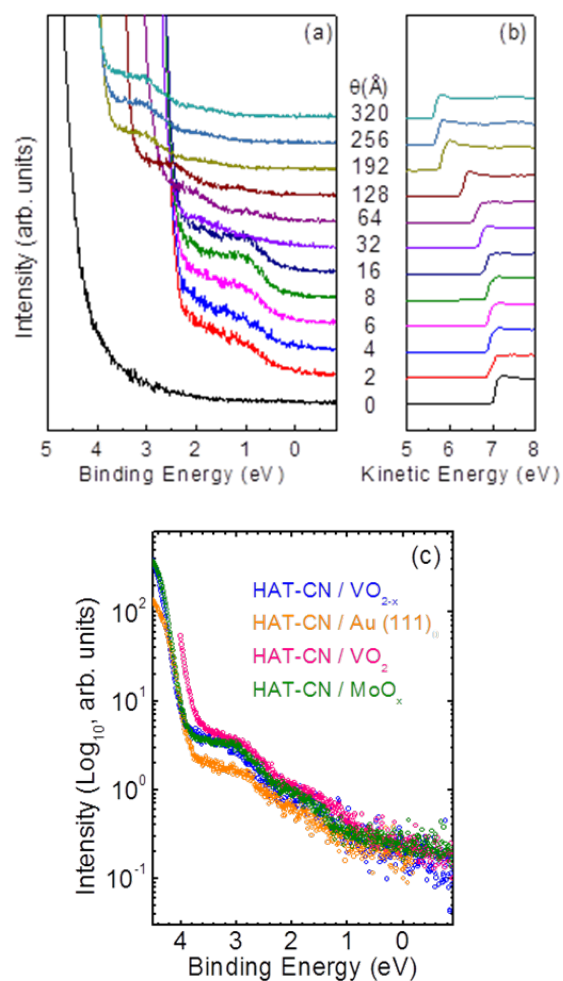
Figure 3 (a) Valence band spectra and (b) SECO region of HAT-CN thin films with increasing nominal thickness (θ) on MoO_x. (c) UPS data of HAT-CN in multilayers on all substrates (nominal thicknesses: 128 Å on VO_2 and VO_{2-x}, 256 Å on Au(111) and 320 Å on MoO_x) .
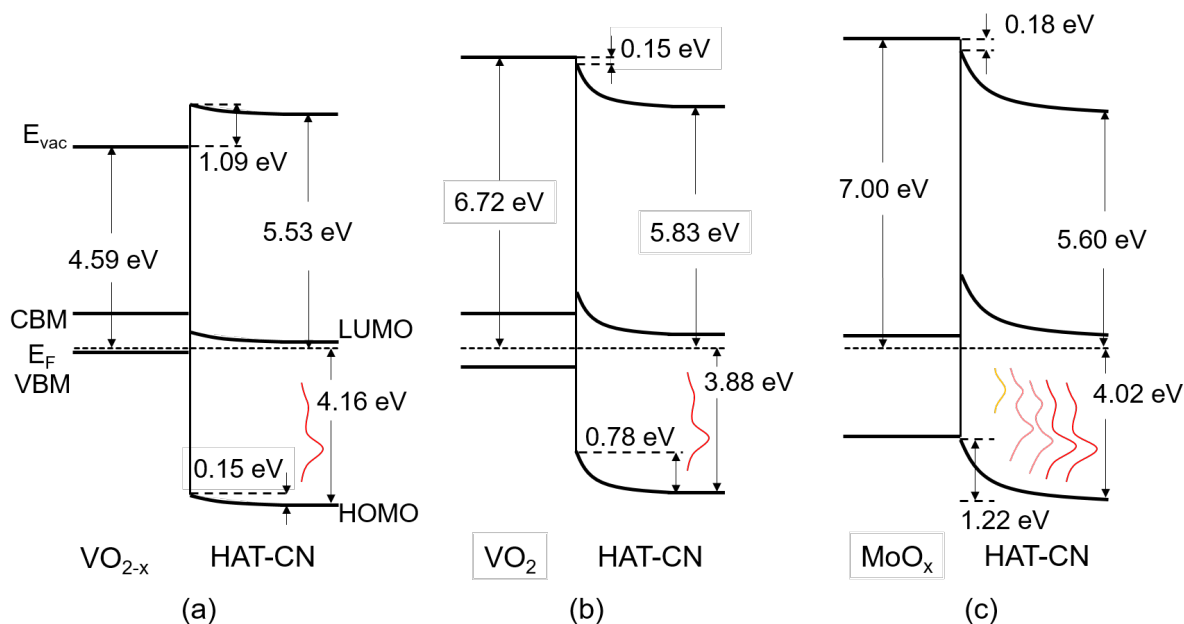
Figure 4 Energy level diagrams of HAT-CN/VO_{2-x} (a), HAT-CN/VO_2 (b) and HAT-CN/MoO_x (c) based on UPS and XPS of this work and the transport gap of HAT-CN (4.24 eV, obtained by IPES [56]). The values for the HOMO-levels are taken from the onsets of the HOMO-derived UPS-peaks for multilayer coverage. The magnitude of the energy-level bending is estimated by the shift of the C1s core-level between nominal HAT-CN thicknesses of 4 Å and 128 Å (320 Å on MoO_x). The gap states for thin HAT-CN coverages could be only observed on MoO_x. However, it is expected that they also exist for ultrathin HAT-CN thin films on VO_{2-x} and VO_2, but are masked by the dominating photoemission intensity of the substrates.

ToC figure

VO$_{2-x}$ HAT-CN   VO$_2$ HAT-CN

4.6 eV   5.5 eV   6.7 eV   5.8 eV
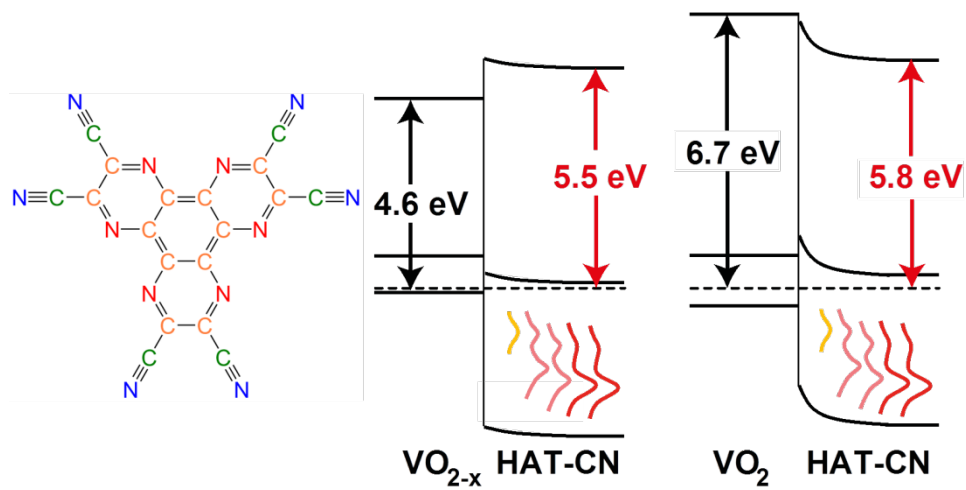
Supporting Information

VO$_2$ and VO$_{2-x}$ substrates
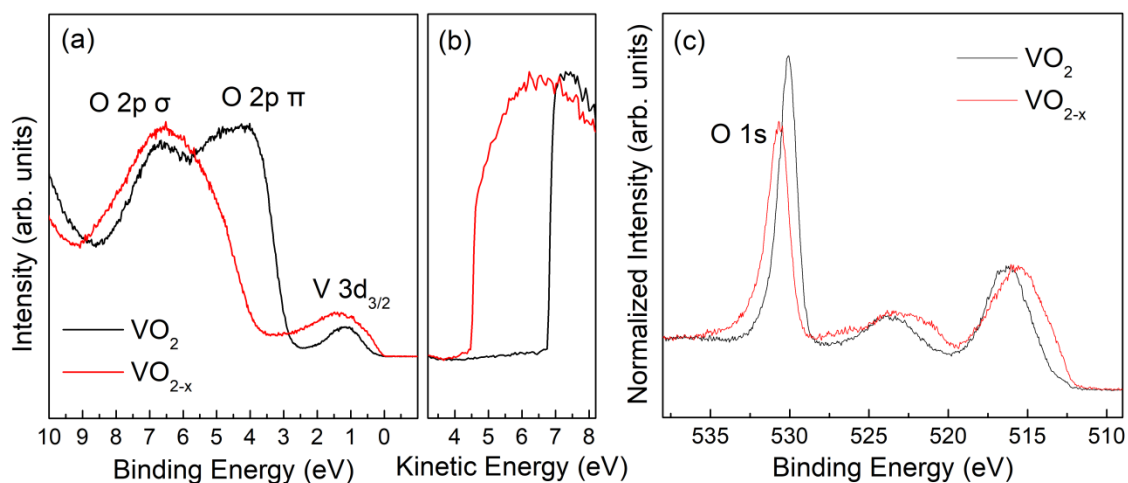
Figure S1 (a) Valence band, (b) SECO and (c) core level regions of VO$_2$ and VO$_{2-x}$ substrates as prepared. In the valence band region of VO$_{2-x}$ components derived from bonding O 2p σ orbitals and from V 3d orbitals are apparent. For VO$_2$, there is an additional peak due to emission from non-bonding O 2p π orbitals. The core level region is normalized by using V 2p$_{3/2}$ as standard reference.

HAT-CN on VO$_{2-x}$ and VO$_2$
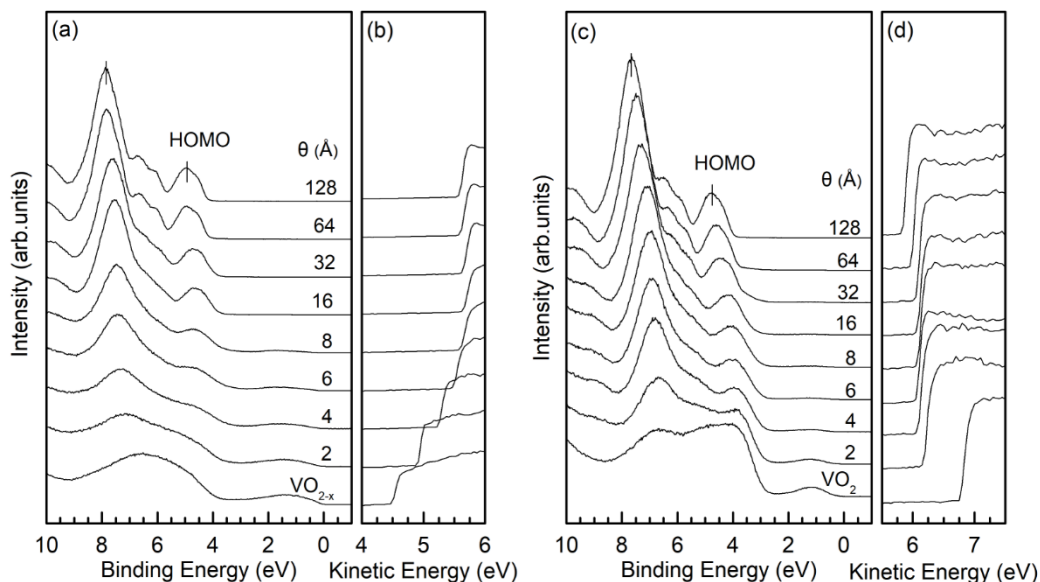
Figure S2 (a) Valence band evolution and SECO evolution by incremental deposition of HAT-CN on VO$_{2-x}$ (a, b) and VO$_2$ (c, d).
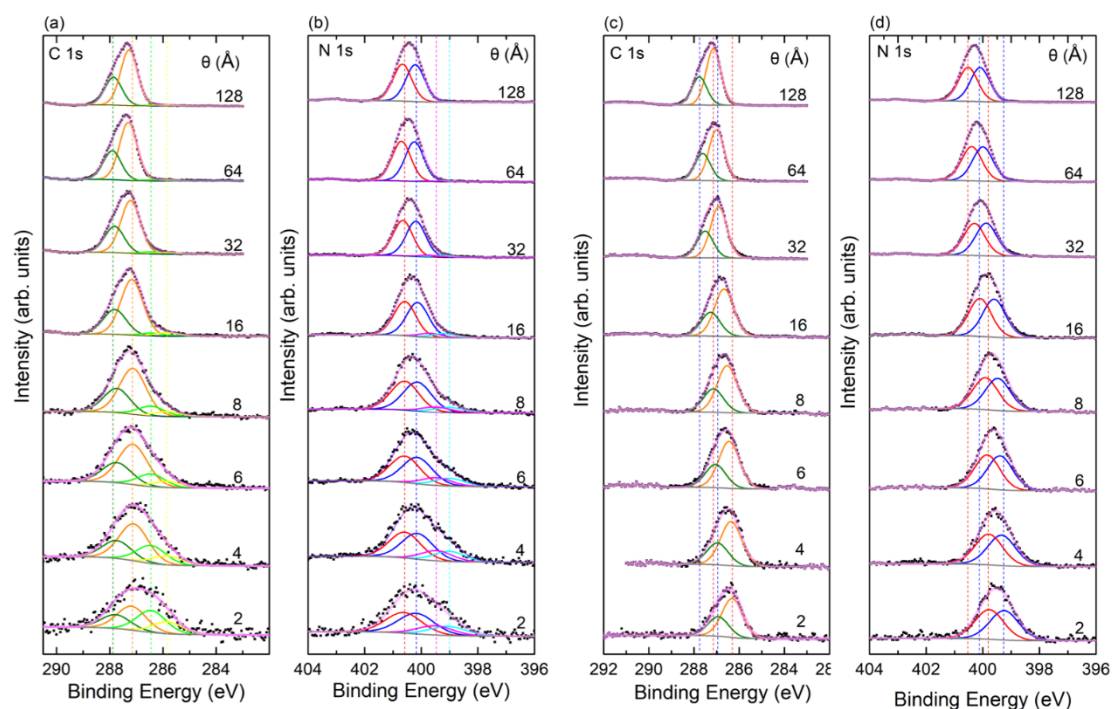
Figure S3 Deconvolution of C1s and N1s emission features of HAT-CN on VO_{2-x} (a, b) and VO_2 (c, d) upon HAT-CN deposition. Carbon atoms in the cyanine groups and in an aromatic environment are colored in olive and orange, respectively, nitrogen atoms in the cyanine groups and in an aromatic environment are colored in blue and red, respectively. The interfacial emission features at low BE sides for both C1s and N1s spectra of HAT-CN on VO_{2-x} (a, b) are shown in light colors, while there are no visible interfacial species observed for HAT-CN on VO_2 (c, d) . The dashed lines in colors are the guides to eye calibrating the corresponding colored components.
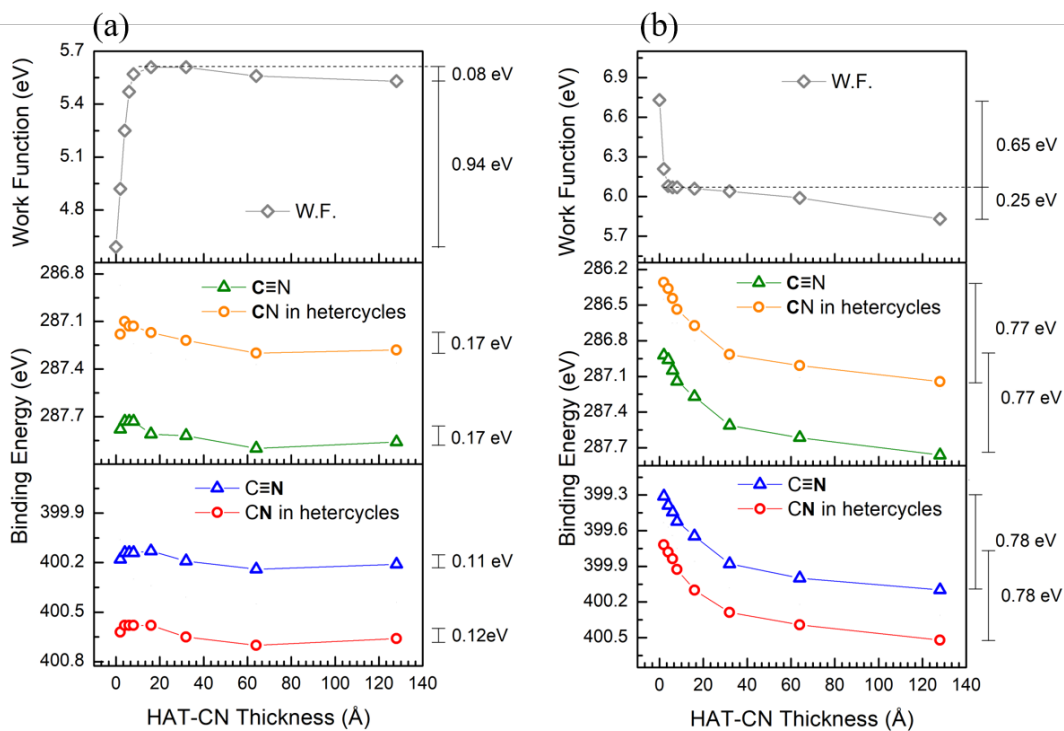
Figure S4 The positions of Φ and core-level BEs for all measured HAT-CN thicknesses on both (a) VO$_{2-x}$ and (b) VO$_2$ are summarized. The change of work function upon HAT-CN deposition is represented in grey diamonds, the carbon and nitrogen components observed in XPS are represented in colored circles and triangles.

HAT-CN on MoO$_x$
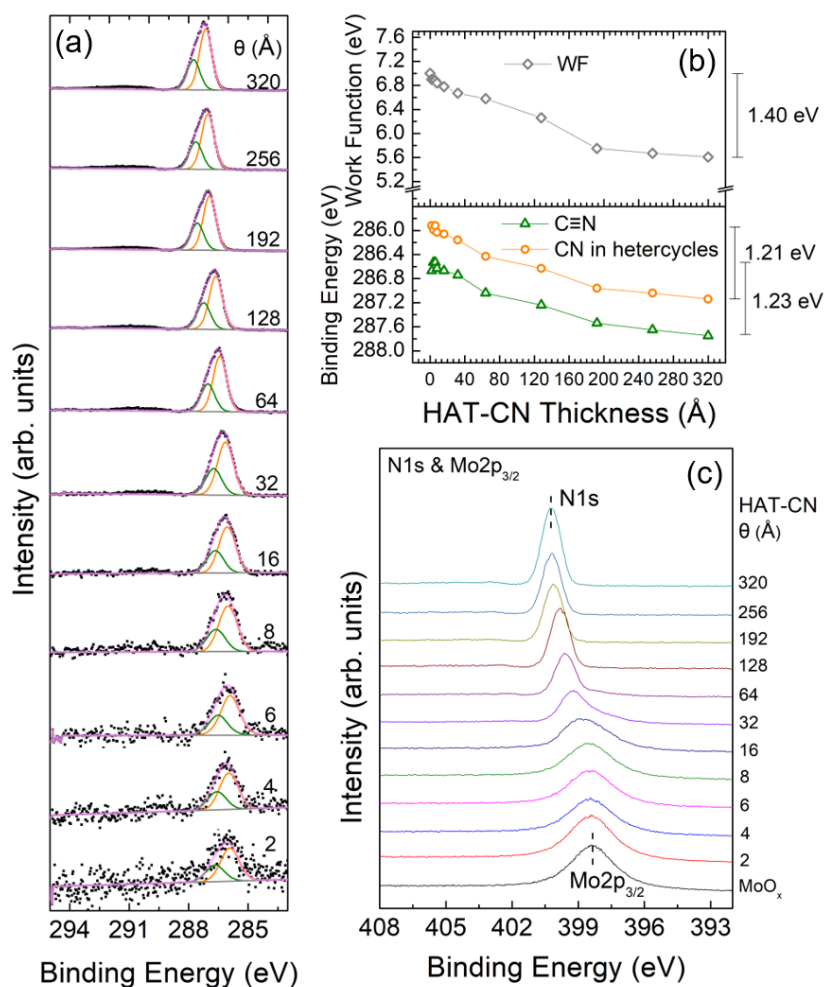
Figure S5 Deconvolution of C1s XPS emission features of HAT-CN/MoO$_x$ (a). Carbon atoms in the cyanine groups and in an aromatic environment are colored in olive and orange, respectively. The positions of Φ and C1s core-level BEs for all measured HATCN thicknesses on MoO$_3$ are summarized in (b); N1s and Mo2p$_{3/2}$ core level evolution (c).
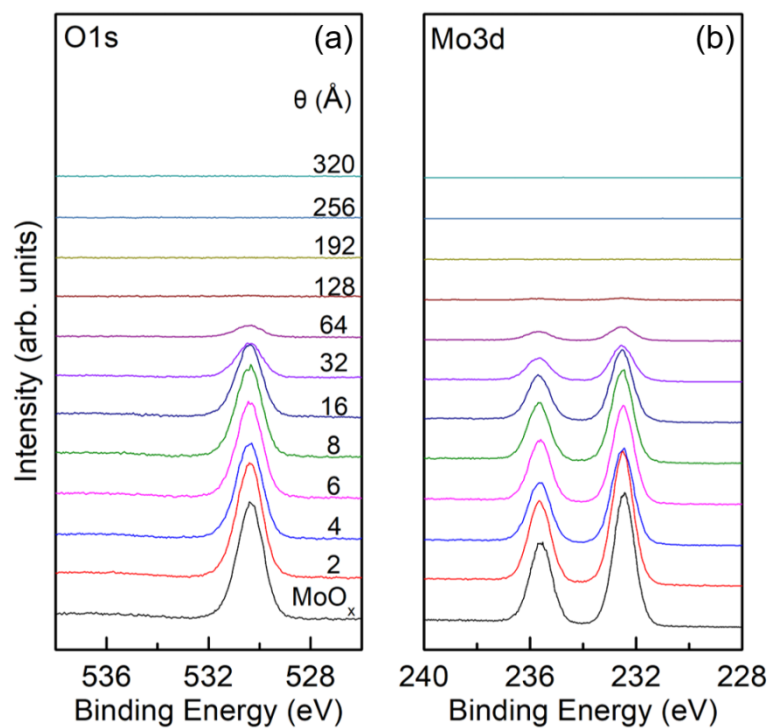
Figure S6 O1s core level evolution (a) and Mo3d core level evolution (b) upon HAT-CN deposition on MoO$_x$. The results illustrate that the X-ray emission features generated from MoO$_x$ substrate are fully covered when the HAT-CN molecular bulk is formed as there is no more substrate signals after 192 Å HAT-CN are deposited on top.

HAT-CN on Au(111)
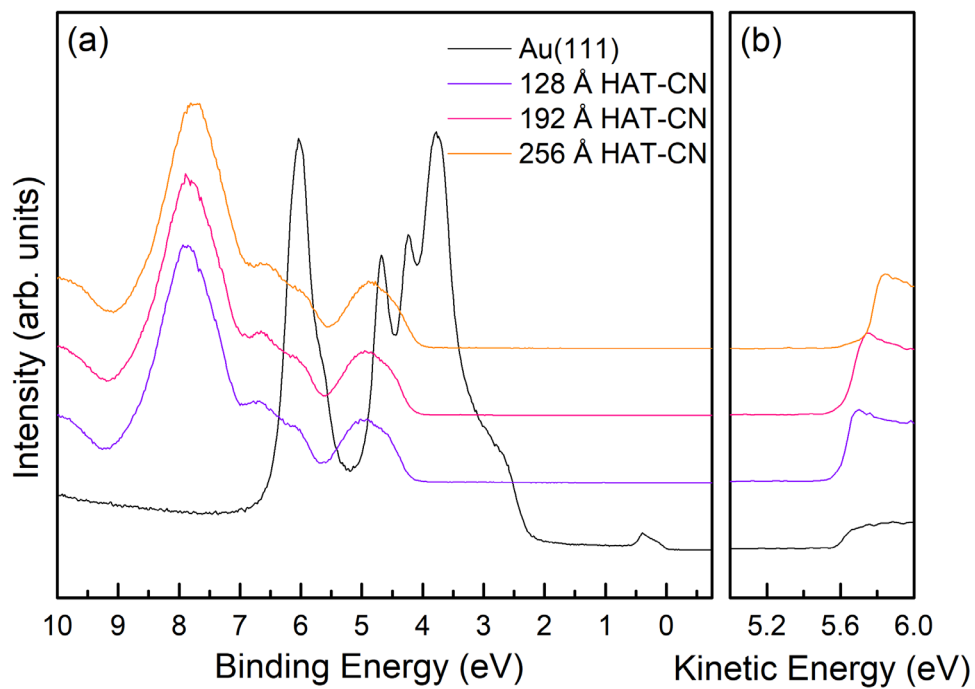
Figure S7 Valence band evolution (a) and SECO evolution (b) upon 256 Å of HAT-CN on Au(111) at normal emission angle.
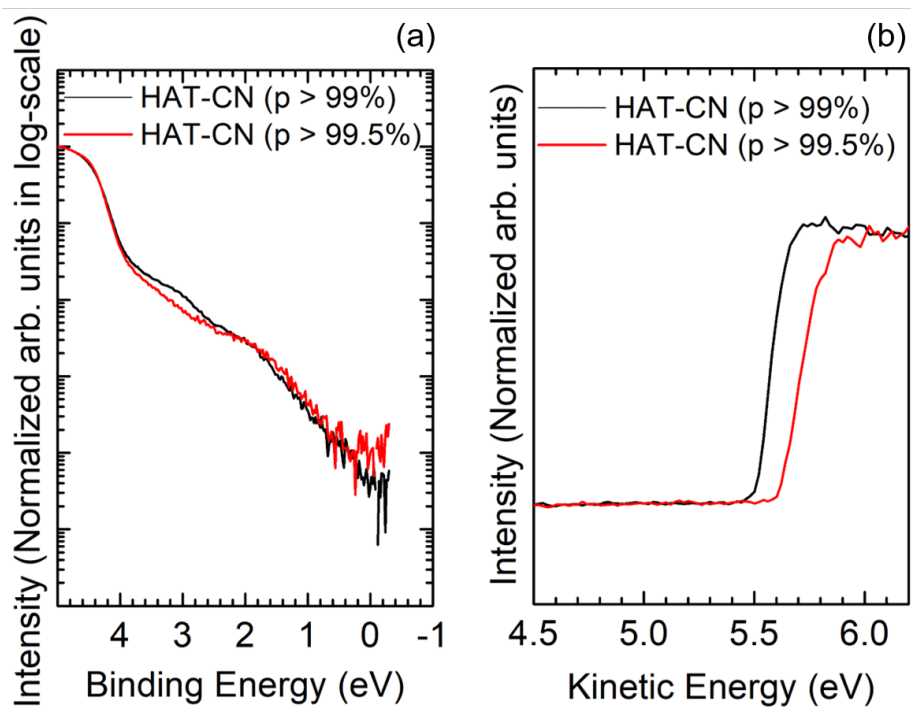
Figure S8 UPS valence electron region (a) and secondary electron cutoff region (b) of HAT-CN thin films on ITO (nominal thickness: 35 nm) with HAT-CN from different suppliers and with different purity (Aladdin 99% and Lumtec 99.5%).